Palaeogeography, Palaeoclimatology, Palaeoecology 436 (2015) 112–122

Contents lists available at ScienceDirect

Palaeogeography, Palaeoclimatology, Palaeoecology

journal homepage: www.elsevier.com/locate/palaeo

Holocene variations in productivity associated with changes in glacier activity and freshwater flux in the central basin of the Strait of Magellan

Claudia Aracena [a,b,*], Rolf Kilian [c,d], Carina B. Lange [b,e], Sebastien Bertrand [f], Frank Lamy [g], Helge W. Arz [h], Ricardo De Pol-Holz [e], Oscar Baeza [c], Silvio Pantoja [b,e], Catherine Kissel [i]

[a] Instituto de Ciencias Marinas y Limnológicas, Universidad Austral de Chile, Campus Isla Teja, Edificio Emilio Pugin, Valdivia, Chile
[b] Centro COPAS, Programa COPAS Sur-Austral, Universidad de Concepción, Casilla 160-C, Concepción, Chile
[c] Lehrstuhl für Geologie, Fachbereich VI, Geowissenschaften, Universität Trier, D-54286 Trier, Germany
[d] Dirección de Programas Antáticos y Subantárticos, Universidad de Magallanes, Avenida Bulnes 01855/casilla 113 D, Punta Arenas, Chile
[e] Departamento de Oceanografía, Universidad de Concepción, Casilla 160-C, Concepción, Chile
[f] Renard Centre of Marine Geology, Ghent University, Krijgslaan 281 S8, 9000 Gent, Belgium
[g] Alfred Wegener Institut für Polar- und Meeresforschung, Am Alten Hafen 26, 27568 Bremerhaven, Germany
[h] Leibniz Institute for Baltic Sea Research Warnemünde, Marine Geology, Seestraße 15, D-18119 Rostock, Germany
[i] Laboratoire des Sciences du Climat et de l'Environnement/IPSL, UMR 8212 CEA/CNRS/UVSQ, Avenue de la Terrasse, 91198 Gif-sur-Yvette Cédex, France

ARTICLE INFO

Article history:
Received 22 January 2015
Received in revised form 16 May 2015
Accepted 18 June 2015
Available online 26 June 2015

Keywords:
Strait of Magellan
Holocene
Paleoproductivity
Thermohaline conditions

ABSTRACT

One of the most important factors controlling fjord primary production in southernmost Patagonia is the variability in the thermohaline structure of the water column. In the present-day environment, thermal stratification is mostly related to freshwater input and in particular, the seasonal melting of glaciers. Here we assess whether this relation between fjord productivity and freshwater input holds true for the Holocene, using a sediment record from the central basin of the Strait of Magellan (core MD07-3132, 53°44.17′S; 70°19.03′W, 301 m). Our approach relies on a proxy-based reconstruction of fjord sea surface temperature (alkenone SST), paleosalinity, freshwater input, and paleoproductivity. The results indicate that, during the early Holocene, the accumulation rate (AR) of marine organic carbon was low (<20 kg m^{-2} kyr^{-1}), most likely due to high freshwater contribution resulting in low salinity and low SSTs. After 8.5 kyr BP and during the mid and late Holocene all the productivity proxies increase. The AR's of marine organic carbon (~30 kg m^{-2} kyr^{-1}), biogenic $CaCO_3$ (~60 kg m^{-2} kyr^{-1}) and biogenic opal (425 kg m^{-2} kyr^{-1}) reached the highest values during the last millennium. This increase was probably driven by the marine transgression where marine macronutrient-rich waters entered into the central basin, while lowered precipitation and decreased meltwater input contributed to increase the basin's SSTs and salinity. The late Holocene rise in productivity was interrupted by a low salinity phase between 3.2 and 2.2 kyr BP, during which productivity returned to early Holocene conditions in response to increased input of glacial clays, as suggested by high values of K/Si ratio (~1.2). Our results indicate that meltwater contribution from glaciers plays a crucial role in controlling fjord productivity on seasonal to millennial timescales.

1. Introduction

The productivity patterns in the fjord system of the Strait of Magellan between 52° and 56°S are mainly influenced by changes in light regime and freshwater input from precipitation and glacier melting, all of which play a role at different timescales from seasonal to millennial. In the Patagonian fjords limnetic and oceanic features overlap generating strong vertical and horizontal physicochemical gradients (e.g., Sievers and Silva, 2008; González et al., 2013). At present, the interaction between the resulting surface freshwater layer and nutrient-rich saline bottom water (mixing and/or stability of the water column) strongly controls primary production fluctuations and species composition (e.g., Saggiomo et al., 1994; Pizarro et al., 2000; Iriarte et al., 2007; Torres et al., 2014). At millennial timescales, the interaction between climate and glacier dynamics could also have affected sea-surface temperature (SST), the thermohaline characteristics of the water column, and consequently paleoproductivity of the Magellan fjord system.

The Strait of Magellan crosses the southern tip of the South American continent from the Pacific Ocean and the hyperhumid southernmost Andes in the west to the semiarid grasslands area and the Atlantic Ocean in the east (Fig. 1). Here, Late Glacial coastline evolution was mainly controlled by glacier dynamics, global sea level rise and the regionally distinct degree of isostatic uplift (Kilian et al., 2013a).

* Corresponding author at: Instituto de Ciencias Marinas y Limnológicas, Universidad Austral de Chile, Campus Isla Teja, Edificio Emilio Pugin, Valdivia, Chile.
E-mail address: claudia.aracena@uach.cl (C. Aracena).

http://dx.doi.org/10.1016/j.palaeo.2015.06.023
0031-0182/

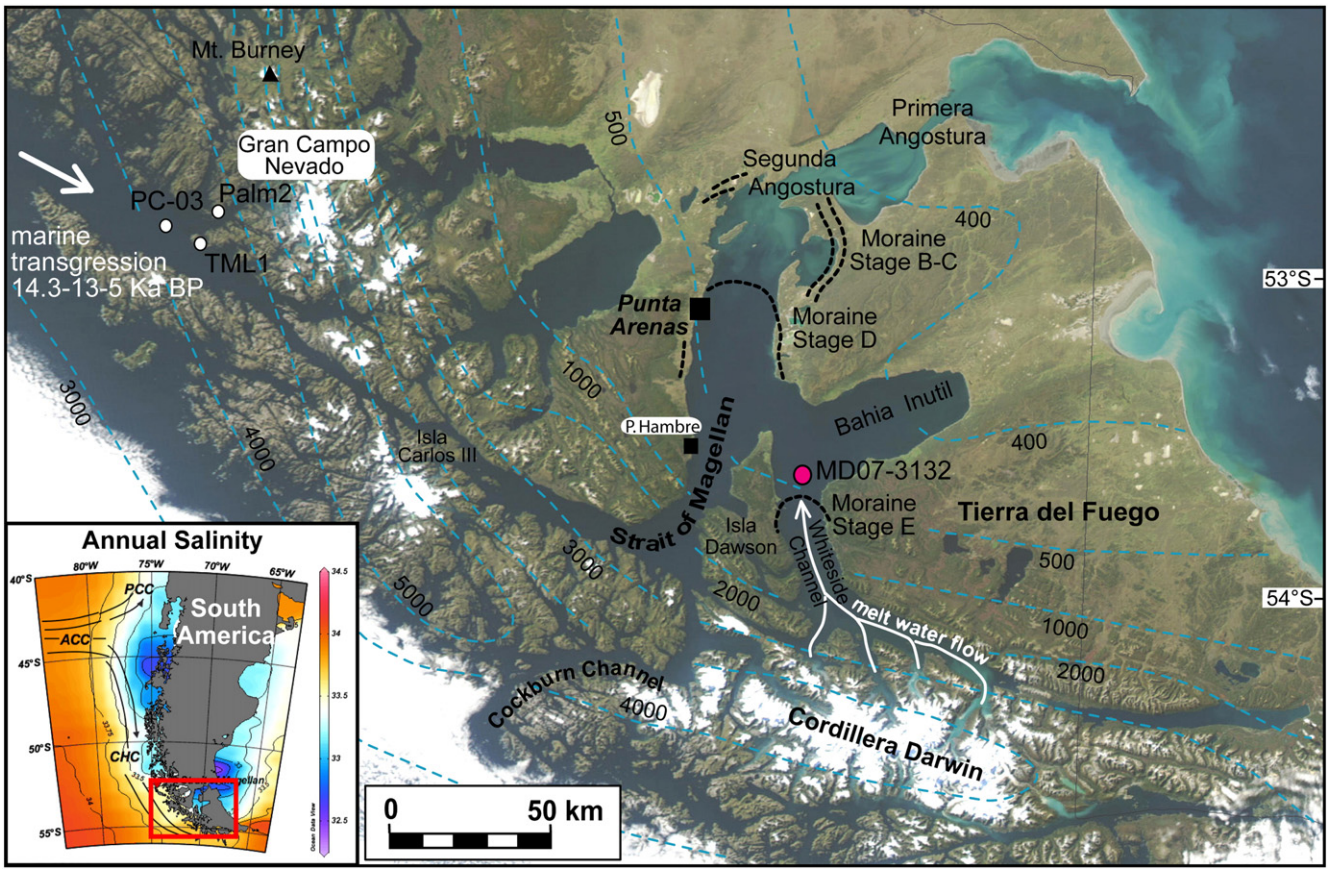

Fig. 1. Map of the Strait of Magellan basin and location of sediment cores MD07-3132 (red dot), PC-03, JPC-67 and TML1 (white dots). The blue dashed lines represent the annual precipitation, which ranges from ~3200 to 9800 mm at the Pacific coast to ~750 mm at the Automatic Weather Stations in the Skyring fjord east of the Andean climatic divide, and to ~500 mm at Punta Arenas (Schneider et al., 2003). The marine transgression for the western entrance is based on Kilian et al. (2007b). The black stippled lines represent moraine stages B–E after McCulloch et al. (2005b) and Bentley et al. (2005a, b). Stage D culminated before 17.7 kyr and reached the latitude of Punta Arenas, and Stage E occurred at 11.7–15.5 kyr BP during which the ice limit reached the northern tip of Isla Dawson (e.g. Bentley et al., 2005a, b; McCulloch et al., 2005a, b; Sugden et al., 2009). The inset figure shows the distribution of surface annual salinity off the coast of Chile (World Ocean Atlas 2009), with less saline waters in the Patagonian fjord region and an increase in salinity towards the open ocean. In addition, the modern surface circulation in the Southeast Pacific off southernmost Chile is shown. CHC: Cape Horn Current; ACC: Antarctic Circumpolar Current; PCC: Peru–Chile Current; SAF: South Antarctic Front.

The influence of environmental conditions and climate on marine productivity during the deglaciation and the Holocene have been mostly investigated for sites located close to the Pacific entrance of the Strait of Magellan (Kilian et al., 2007a; Kilian and Lamy, 2012; Harada et al., 2013), but no detailed studies have been published for the central basin of this fjord system.

This study focuses on sediment core MD07-3132 from the Whiteside Channel (Fig. 1), which belongs to the central basin of the Strait of Magellan. This site is mainly influenced by calving glaciers form Cordillera Darwin that produce a nutrient-poor freshwater supply that is modified by regional precipitation, most likely linked to the Southern Westerly winds (SWWs) (Lamy et al., 2010). During the Holocene, the strength and direction of these winds together with deglaciation and the marine transgression may have further influenced the thermohaline conditions that in particular controlled paleoproductivity. Sediment cores from the western Strait of Magellan suggest a marine transgression at ~14.3 kyr BP (Kilian et al., 2007a, b). In the central Strait of Magellan, Sugden et al. (2005) and McCulloch et al. (2005a, b) proposed the existence of a proglacial lake during the Late Glacial formed by an ice dam lake near Segunda Angostura (Fig. 1). The thermohaline structure and circulation in these environments and associated sediment transport are widely unexplored and may have changed fundamentally after the marine transgression (Kilian et al., 2007a, b; Kilian and Lamy, 2012).

The current knowledge of Late Glacial and Holocene-temperature conditions in southern Patagonia is based on a limited number of SST reconstructions from the Chilean continental margin at 41°S (Kaiser et al., 2005; Lamy et al., 2007) and at 53°S (Caniupán et al., 2011; Siani et al., 2013). Further temperature records are available from the South Atlantic at 53°S (Bianchi and Gersonde, 2004), as well as DOME C Antarctic ice core temperatures (EPICA Community Members, 2004). These records reveal an early Holocene climate optimum between 12 and 8 cal kyr BP that follows the Antarctic Cold Reversal. This warm phase had ~2 °C SST higher compared to the late Holocene and was accompanied by a southward shift in the SWWs with an intensified core between 50 and 55°S (Lamy et al., 2010). On the other hand, the westerly-related increased precipitation and melting of glaciers during summer and especially during the early Holocene may have caused lower salinities and comparatively lower SSTs (Caniupán et al., 2014). The effect of these Holocene changes in temperature and precipitation on aquatic bioproductivity remains however relatively unknown. Here we use a multi-proxy analysis of sediment core MD07-3132 to estimate the influence of changes in temperature, precipitation and marine transgression on paleoproductivity throughout the Holocene. More specifically, our approach is based on a proxy-reconstruction of fjord sea surface temperature (alkenone SST), paleosalinity (chlorine to water content ratio and accumulation rate [AR] of biogenic carbonate), freshwater input (chemical signature of allochtonous glacial clay, AR of terrestrial organic carbon and siliciclastics), and paleoproductivity (AR of marine organic carbon, biogenic opal and carbonate).

2. Material and methods

2.1. Study area

The fjords of southernmost Patagonia are influenced by seasonal and latitudinal changes in precipitation, which is nearly entirely controlled by the regional distribution and intensities of the SWWs (Garreaud et al., 2013). These winds have a summer maximum over southernmost Chile (e.g., Schneider et al., 2003; Lamy et al., 2010) and during austral summer they are more confined and intensified between 50–55°S around the Strait of Magellan area (Fig. 1). Furthermore, the morphology of this region causes strong variations in annual mean precipitation ranging from 5000–10,000 mm yr^{-1} at the climate divide to less than 300 mm yr^{-1} farther to the east, producing one of the most dramatic precipitation gradients on Earth (Garreaud et al., 2013; Fig. 1). Due to the strong orogenic effect of the Southern Andes, a season with stronger SWWs will increase (decrease) local precipitation at any latitude in western (eastern) Patagonia (Garreaud et al., 2013). Due to predominant westerly winds, it is likely that a large amount of surface freshwater is transported eastward towards the central section of the Strait of Magellan and finally into the Atlantic where it forms an extended low salinity anomaly (Fig. 1, inset; Acha et al., 2004). In particular, during austral spring and summer these fjords receive a high amount of freshwater from annual precipitation/or glacier melting, causing a low salinity surface layer that is relatively stable and discharges to the open ocean (Dávila et al., 2002). Nutrient-rich marine water enters at the bottom of these fjords, but may be hampered by the complex bathymetry, including several shallow sills (Kilian et al., 2007a; Araya-Vergara, 2008). Here, the thermohaline structure in the water column depends primarily on the amount of regional freshwater supply and the degree of mixing with the underlying marine waters, which strongly depends on the orientation of the fjord towards the local wind system (Valdenegro and Silva, 2003). Clay bearing meltwater plumes influence the light regime in the surface water layer (Silva, 2008) limiting photosynthetic processes for phytoplankton.

The Strait of Magellan is a 575-km long and up to 1200 m deep fjord system that separates continental South America from Tierra del Fuego. It encompasses an area of ~132,000 km^2 (Fig. 1) and was formed by sub-bottom erosion of large temperate glacier systems during the Pleistocene (Araya-Vergara, 2008) partly following NWW–SEE trending fracture zones (Breuer et al., 2013). The central Strait of Magellan forms a branched basin with 30 to 40-m sills of Primera and Segunda Angostura in the north, and the 80-m deep sill of Isla Carlos III in the west (Fig. 1). These sills control the inflow of marine bottom water (Valdenegro and Silva, 2003) and have controlled the timing and degree of the marine transgression in the past (Kilian et al., 2007a; Kilian et al, 2013a, b).

Thermohaline and nutrient characteristics along the Strait of Magellan have been compiled and are illustrated in Fig. 2 using data of CIMAR 3 FIORDOS cruise of spring 1998. The vertical structure of the water column in the western basin is typical for estuarine conditions, with a relatively cold surface layer (<7 °C), low salinity (<28 psu), and high oxygen content (~7 mL/L) in the upper 50 m (Fig. 2). Subsurface and deeper layers (down to ~800 m), in turn, are more homogeneous, warmer (>9 °C) and saltier (>32), and are associated with a net flow of SAAW and the relatively warm CHC from the Pacific Ocean (Valdenegro and Silva, 2003). The 80 m deep sill near the Carlos III island hampers the eastward intrusion of SAAW into the central section of the Strait (Valdenegro and Silva, 2003). Thus, the thermohaline structure is different in the central basin; the water column is less stratified (with average annual temperatures ranging between 7 and 8 °C, and salinities between 30 and 31) (Fig. 2). However, between Whiteside Channel and Bahía Inútil a comparatively cold meltwater-derived tongue (~6 °C) at 100 m depth extends into the central basin. Oxygen content is also rather homogenous in the central basin (~6.5 mL/L) and increases towards the more freshwater-influenced southern Bahía Inútil and Whiteside Channel (7 mL/L; Fig. 2, upper three panels).

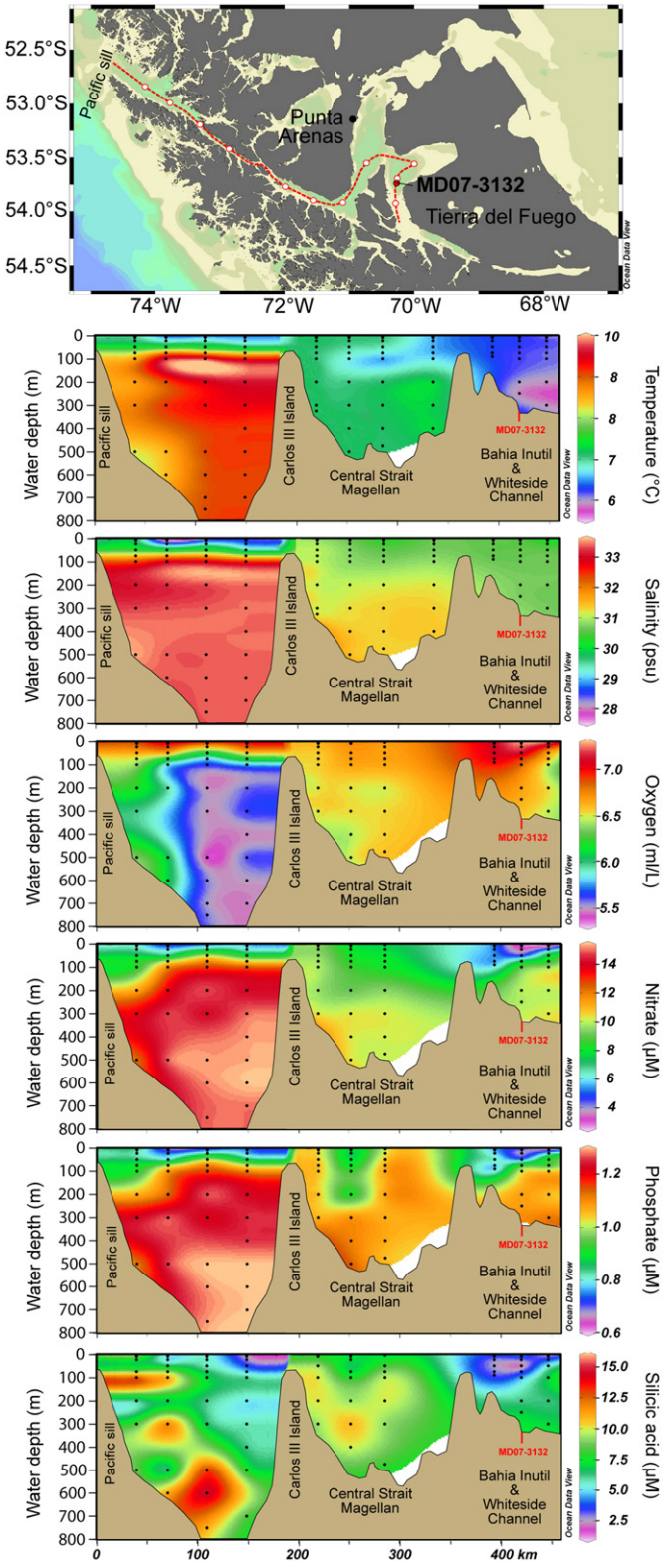

Fig. 2. Present day horizontal and vertical distributions of temperature, salinity, oxygen and nutrients in the water column along a W–E section of the Strait of Magellan from the Pacific entrance to the Whiteside Channel where core MD07-3132 is located. Data refer to austral spring 1998 and were obtained from CIMAR 3 FIORDO reports (http://www.shoa.cl/n_cendhoc/productos/cimar-3/index.html). Blank spaces: no data. The gray polygon represents the bathymetry of the W–E section.

Fig. 2 illustrates the freshwater influence of proglacial rivers and precipitation from elevated mountains at the eastern and western ends of the profile.

The vertical distribution of macronutrient concentrations in the water column also has distinctive patterns for each basin (Fig. 2, lower three panels). In the western basin the upper 100-m layer is characterized by concentrations of nitrate ranging 5–8 μM, phosphate 0.6–0.8 μM and silicic acid 2.5–7 μM. Below 100 m depth the water column becomes more enriched in nitrate and phosphate concentration (>10 μM and >1 μM, respectively). The vertical distribution of silicic acid in subsurface and deep waters is very heterogeneous, reaching 15 μM on the western flank and about 7.5 μM near Carlos III Island. Nutrients in the central basin change more gradually with depth, with lower values in the upper layers (~7.5 μM for nitrate, <1 μM for phosphate, and 7.5 μM for silicic acid) than at depths below 200 m (~11 μM, >1 μM, and ~10 μM, respectively). As was the case for the thermohaline structure, the surface layer in the Whiteside Channel and Bahía Inútil areas has a distinct pattern with extremely low concentrations of all nutrients (Fig. 2).

2.2. Sediment coring and lithology

Sediment core MD07-3132 was retrieved from 301 m water depth in the Whiteside Channel, which is located at the northeastern corner of Isla Dawson and close to the southern end of Bahía Inútil (53°44.17′S, 70°19.03′W; Fig. 1). The core is 2173 cm long and was obtained with a Calypso piston corer during IMAGES (International Marine Past Global Changes Studies) XV-MD159-Pachiderme cruise on board R/V *Marion Dufresne* (French Polar Institute, IPEV) in February 2007. The sediment core was split and described onboard with respect to its macroscopic characteristics, using smear slides. Core logging onboard included magnetic susceptibility and color scanning (Kissel, 2007a). The lowermost section of the core below 1500 cm corresponds to a diamicton facies characterized by the presence of abundant dropstones and cm-thick laminae and the lack of biogenic components (Kissel, 2007a, b). Towards the top of the core (above 1500 cm) sediments gradually change to a more organic-bearing facies. Three tephra layers were identified at 592–600 cm, 1060 cm, and 1248 cm (see Supplementary information, Figs. S1 and S2).

2.3. Chronology

The chronology of sediment core MD07-3132 is based on ten radiocarbon ages and three known tephra layers. Shell fragments of molluscs, scaphopods, and calcareous worm tubes were selected for radiocarbon dating since foraminifera were scarce throughout the core and absent below 1600 cm (see Supplementary information, Figs. S1 and S2). No shell fragment suitable for dating was found below 1475 cm. AMS radiocarbon ages were determined at the National Ocean Sciences Accelerator Mass Spectrometry Facility (NOSAMS, Woods Hole Oceanographic Institution) and at the Department of Earth Systems Sciences, University of California Irvine (Table 1). Radiocarbon ages were calibrated with CLAM 2.2 (Blaauw, 2010), using the calibration curve SHCal13 (Hogg et al., 2013). In addition to the radiocarbon ages, the Mt Burney MB2 tephra (4150 ± 50 yr BP; McCulloch and Davies, 2001; Kilian et al., 2003; Stern, 2008) was recognized at 592–600 cm. The two other tephras (1060 cm and 1248 cm) were interpreted as the Hudson H1 (8020 ± 250 yr BP) and Mt Burney MB1 (9050 ± 200 yr BP), in agreement with their distribution maps and individual textures (Kilian et al., 2003; Stern, 2008), and with their estimated age in the sediment core. A reservoir age of 600 years was estimated from the age difference between the MB2 tephra and the radiocarbon ages. For the interpretation of our results we have used the formal subdivision of the Holocene Series/Epoch proposed by Walker et al. (2012).

Table 1
Radiocarbon ages obtained from sediment core MD07-3132.

Core depth (cm)	Laboratory code	Material	^{14}C yr BP ± 1σ	2σ calibrated range
112	OS-82053	Bivalve	1075 ± 15	488–514
120	OS-82054	Calcareous worm tube	1220 ± 15	542–629
230	OS-82055	Calcareous worm tube	1915 ± 15	1178–1270
405	UCIAMS-72976	Mollusc	3200 ± 30	2495–2754
620	OS-72977	Mollusc	4530 ± 35	4159–4421
688	OS-82056	Scaphopod	4945 ± 15	4830–4959
850	OS-82057	Bivalve	6105 ± 15	6210–6303
998	UCIAMS-72978	Mollusc	7480 ± 55	7582–7790
1220	OS-72979	Mollusc	8710 ± 40	8776–9121
1475	OS-72980	Mollusc	9990 ± 40	10,427–10,695

All radiocarbon ages were calibrated with CLAM 2.2 (Blaauw, 2010), using the SHCal13 calibration curve, and after application of a reservoir age correction of 600 years. OS = National Ocean Sciences Accelerator Mass Spectrometry Facility (NOSAMS, Woods Hole Oceanographic Institution, MA, USA); UCIAMS = Department of Earth Systems Sciences University of California, Irvine, CA, USA.

2.4. Geochemical and sedimentological analyses

The chemical composition (Si, Cl, and K) of sediment core MD07-3132 was measured directly at the surface of the split core at 1-cm resolution with an Avaatech™ X-Ray Fluorescence (XRF) Core Scanner at the Alfred Wegener Institute (AWI) in Bremerhaven, Germany. This non-destructive measuring technique allows semi-quantitative geochemical analysis of split sediment cores (Ritcher et al., 2006). Measurements were carried out at 10 kV.

The contents of total carbon and total nitrogen were determined with an elemental analyzer VARIO Element III at the AWI, Bremerhaven. Samples were taken every 8 cm (age resolution between 39 and 74 years), and measurements were done on 5 mg of freeze-dried sediment placed in tin capsules. Estimated detection limits are 0.01 wt.% for carbon, and 0.02 wt.% for nitrogen. The organic carbon (OC) content was determined on a LECO Carbon Sulfur Analyzer (LECO-CS 125) at the AWI, Bremerhaven. The measurements were made with a resolution of 8 cm in sediments previously freeze-dried, homogenized and acidified by direct addition of 1M HCl, and dried overnight at 150 °C. Terrestrial and marine organic carbon ($_{terr}$OC and $_{mar}$OC, respectively) were calculated from OC contents using molar N to C ratios (Perdue and Koprivnjak, 2007). We used a molar N/C = 0.17 as the marine (microalgal) end-member (Meyers, 2003) and N/C = 0.055 as our terrestrial (vascular plant) end-member, which is based on the average values from sediment samples of rivers Gallego and Marinelli (Sebastien Bertrand, unpubl. data). Carbonate contents were calculated from the difference between the amount of total carbon and organic carbon as $CaCO_3 = (\text{total C} - \text{OC}) \times 8.333$.

Samples for biogenic opal and total alkenone contents, and alkenone-based SST ($U^{K'}_{37}$) were taken with a resolution of 16 cm. Sample preparation and measurements were done at the laboratories of Paleoceanography and Marine Organic Geochemistry, Universidad de Concepción, Chile. Biogenic opal was estimated following the procedure described by Mortlock and Froelich (1989) and modified by Müller and Schneider (1993) using the molybdenum blue method. Biogenic Si (Si_{OPAL}) = 112.4 × (Cs/M), where Cs = silica concentration in the sample (nM), M = sample mass (mg), and 112.4 = atomic weight of Si (28.09 g × mol^{-1}) × the extraction volume of NaOH (0.04 L) × 100. We converted $\%Si_{OPAL}$ to %biogenic opal according to the equation $\%OPAL = 2.4 \times \%Si_{OPAL}$ (Mortlock and Froelich, 1989).

C-37 alkenone contents and paleotemperatures (SST °C) were estimated following the method of Prahl and Wakeham (1987). Total alkenone contents were calculated as the sum of di, tri and tetra-unsaturated C_{37} alkenones and expressed in μg/g. The concentrations were estimated with a Shimadzu gas chromatographer with a capillary column (Rtx-5 m, 0.22 μm; 0.32 mm i.d. × 30m, J & W Scientific) and a

flame ionization detector. SST was calculated using the linear calibration function relating the unsaturation index $U^{k'}_{37}$ to growth temperature T as $U^{k'}_{37} = 0.033T + 0.043$ (Prahl and Wakeham, 1987).

Biogenic proxies OC, $CaCO_3$ and opal are also reported as accumulation rates (AR in kg m^{-2} kyr^{-1}). Calculations were based on multiplying contents of each proxy by dry bulk density and sedimentation rate for each sampling interval.

Percentages of siliciclastic material were calculated as 100 wt.% − ($CaCO_3$ wt.% + 2 × OCwt. % + biogenic opal wt.%) (e.g., Bertrand et al., 2012).

In this study, AR of $_{mar}$OC, $CaCO_3$ (as a proxy for calcareous microorganisms, i.e., coccolithophorids and foraminifera) and biogenic opal (as a proxy for siliceous microorganisms, mainly diatoms) were used to reconstruct paleoproductivity in the central section of the Strait of Magellan. Siliciclastic material and $_{terr}$OC were used as freshwater input proxies since both primarily originate from nearby land sources and are supplied to the study site during strong rainfall periods or meltwater plumes. The reconstruction of the environmental conditions of the area is based on alkenone-derived SST and the K/Si ratios (used as a proxy of glacial clay input from the granitoid catchment of the Andean glaciers, SERNAGEOMIN, 2003). Paleosalinity changes were inferred from the chlorine to water content ratio (Cl/Water %; calculated as XRF chlorine counts divided by the pore water content; see Supplementary information, Fig. S3). In addition, biogenic carbonate fluctuations may also reflect salinity changes, as suggested by Kilian et al. (2013a) for fjord sites ~ 53°S.

3. Results

3.1. Sediment composition

Sediment core MD07-3132 (Fig. 3) is dominated by siliciclastic material, ranging between 77 and 97 wt.% (Fig. 3a). The average siliciclastic content is 89% below 1250 cm, and it decreases to 84% for the upper part of the core (above 1250 cm). Organic carbon content is lowest at the base of the core (0.7 ± 0.2 wt.% at ~22 m) increasing gradually towards younger sediments and reaching 1.2 ± 0.3 wt.% at the top of the core; this trend is disrupted by a sharp decline at 576–592 cm (Fig. 3b). Low, albeit highly variable $CaCO_3$ contents characterize the deepest section of the core (below 1720 cm; 0.03–1.6 wt.%) followed by a continuous increase towards the top (from ~1 to 3.3 wt.%) which is interrupted by a sudden decline at 376–476 cm (Fig. 3c). Opal content is highly variable along the core (3–18 wt.%), especially above 1400 cm (Fig. 3d). The C/N molar ratio ranges between 5 and 8, with the exception of a marked drop at 632–648 cm (Fig. 3e). The lowermost 3 m of the core are characterized by the highest glacial clay input (K/Si ratio > 1.5; Fig. 3f), high amounts of coarse clastic mineral particles (>150 μm; >10–47 wt.%; Fig. 3g), and both characteristics coincide with the highest magnetic susceptibility signal (Fig. 3h). In these basal sediments alkenones are completely absent until ~1800 cm in accordance with a diamicton facies with dropstones (see Supplementary information, Fig. S2). Thereafter, alkenones occur intermittently until 1120 cm and then become continuous towards the top of the core (Fig. 3i).

3.2. Chronology and sedimentation rates

Sediment core MD07-3132 covers the entire Holocene and parts of the Late Glacial. However, the lowermost radiocarbon age (10,430–10,695 cal yr BP) was obtained at 1475 cm, and the 1475–2173 cm section did not contain any material for ^{14}C dating. Thus, the chronology was not extrapolated below 1500 cm depth because sediment composition in the lower part of the core represents a more glacier-proximal facies, which could be characterized by higher AR (see Supplementary information, Fig. S2). The final chronology is restricted to the Holocene and consists in a smooth spline (smooth factor: 0.3) fitting through the probability distributions of the calibrated radiocarbon ages and the calendar ages of tephras H1, MB1 and MB2 (Table 1; Fig. 4). A smooth spline (smooth factor: 0.3) is preferred over linear regressions since there are no visible features in the sediment core that indicate abrupt changes in AR. The Holocene sedimentation rates range from 1.1 to 2.0 mm yr^{-1}, with an average of 1.4 mm yr^{-1}. The sedimentation rates are highest (>1.5 mm yr^{-1}) before 8000 cal yr BP (Fig. 4).

3.3. Holocene changes in paleoproductivity and sources of organic carbon

During the early Holocene accumulation rates of marine organic carbon and biogenic carbonate are low (AR $_{mar}$OC < 20 kg m^{-2} kyr^{-1} and AR $CaCO_3$ ≤ 40 kg m^{-2} kyr^{-1}; Fig. 5a and b, respectively). Biogenic opal, on the other hand, fluctuates widely between ~300 kg m^{-2} kyr^{-1} (at 10 and 8.5 kyr BP) and <100 kg m^{-2} kyr^{-1} (at ca. 9.5 kyr BP) (Fig. 5c). This drop coincides with the lowest values in the Cl/Water % (≤75; Fig. 5g) and highest K/Si ratios (Fig. 5f). Also in the early Holocene, AR of $_{terr}$OC and siliciclastic material are high (≥5 kg m^{-2} kyr^{-1} and >1800 kg m^{-2} kyr^{-1}, respectively; Fig. 5d, e). Alkenone-derived SSTs drop below 7 °C (5.4 °C at 9.6 kyr BP; Fig. 5h) although the record is interrupted between ~9.5 and 8.5 kyr BP due to the absence of alkenones (1312–1136 cm; Fig. 3g).

During the middle Holocene (8.2–4.2 kyr BP) ARs of $_{mar}$OC and biogenic $CaCO_3$ slightly increase and the AR of biogenic opal decreases (Fig. 5a, b, c). The AR of siliciclastic material shows a 40% decrease compared to the early Holocene, and AR $_{terr}$OC approaches cero (Fig. 5d, e). In addition, the K/Si remains relatively stable (around 0.9). These fluctuations are accompanied by a progressive and continuous rise in the Cl/Water % (from 85 to 140 Cl/Water %; Fig. 5g) and an increasing trend in our alkenone-derived SSTs (from ~8 to 10.5 °C; Fig. 5h).

The late Holocene, after 4.2 kyr BP, is characterized by a general increase in the AR of all paleoproductivity proxies (Fig. 5 a, b, c) reaching maximum values for $_{mar}$OC (~30 kg m^{-2} kyr^{-1}), biogenic $CaCO_3$ (~60 kg m^{-2} kyr^{-1}) and biogenic opal (425 kg m^{-2} kyr^{-1}) in the last millennium. The rise in productivity proxies is accompanied by a gradual increase in ARs of $_{terr}$OC (from 0 to ~14 kg m^{-2} kyr^{-1}) and siliciclastics (from 1200 to ~2200 kg m^{-2} kyr^{-1}) (Fig. 5 d, e) whereas K/Si and Cl/Water % remain rather stable. Late Holocene SSTs fluctuate around 9 °C and reach 10.9 °C at ~2.1 kyr BP. This is followed by SSTs ~ 8 °C except for a short peak of 9.9 °C at 0.8 kyr BP (Fig. 5h).

4. Discussion

Thermohaline conditions, nutrient availability, and daily irradiance are the most important factors controlling present-day bioproductivity in the Chilean fjords (e.g., Iriarte et al., 2007; Aracena et al., 2011; González et al., 2011; Torres et al., 2011). Although some nutrients (like iron and dissolved silicon, and terrestrial organic carbon including nitrogen and phosphorus) may be derived from local terrestrial sources, it is the ocean water that plays the most important role for the input of macronutrients. However, the extension of the surface nutrient-poor freshwater layer depends on precipitation-related runoff and glacier/snow melting which changes seasonally. This seasonality may have changed considerably during the Holocene (e.g., Lamy et al., 2010).

The mixing of the deeper more saline and nutrient-rich fjord water with the fresher surface water is governed by density contrasts (i.e. temperature and salinity), wind-induced currents, tides, and total residence time of the water masses in the fjord system (e.g., Antezana, 1999; Valdenegro and Silva, 2003; Valle-Levinson et al., 2006; Torres et al., 2011). The long-term (centennial–millennial) changes in the thermohaline conditions and productivity in the Strait of Magellan are poorly understood but can be reconstructed using sediment proxies. In the following sections we discuss the influence of freshwater flux on productivity as a response to Holocene glacier fluctuations, marine transgression and coastline evolution in the central basin of the Strait of Magellan.

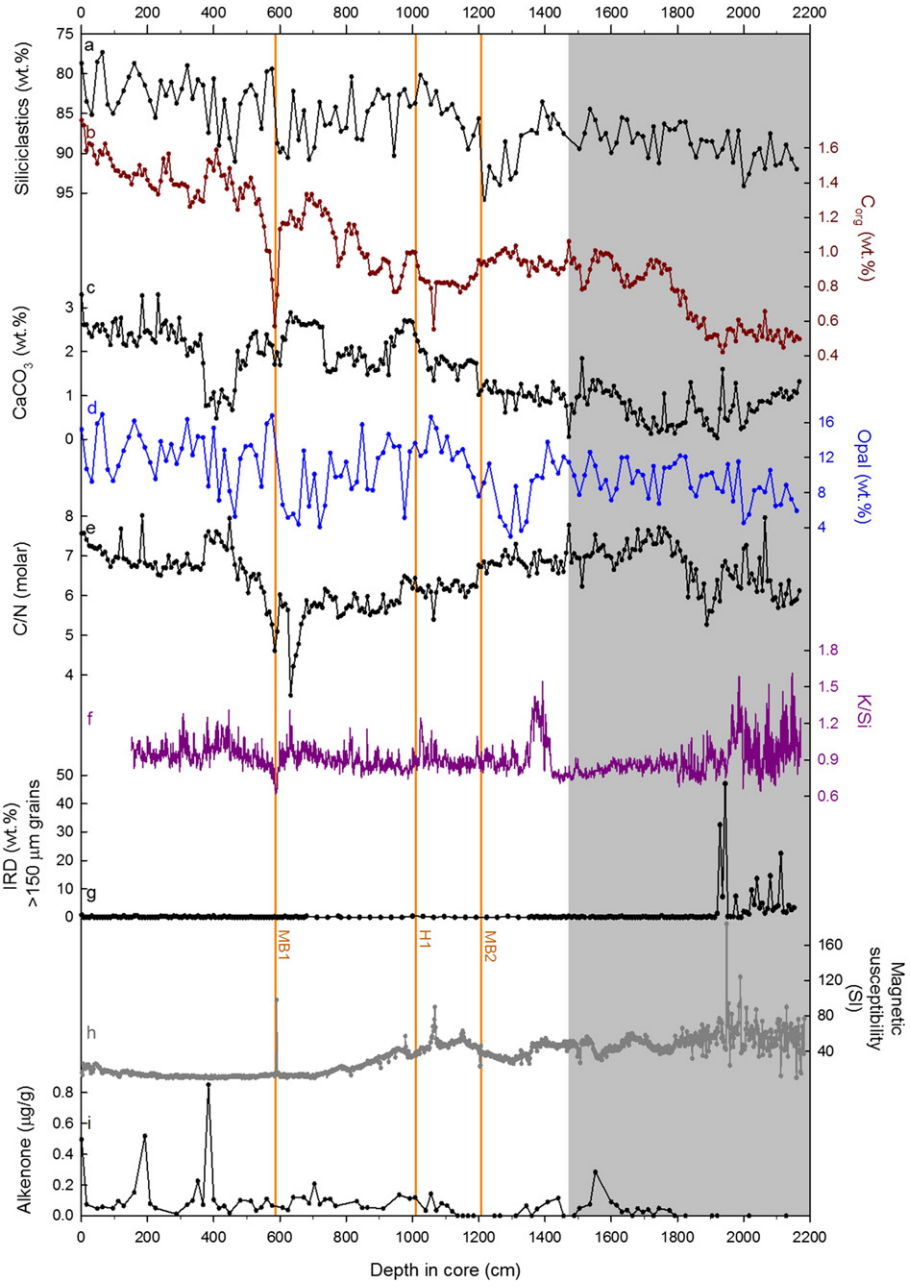

Fig. 3. Sediment composition vs depth in core MD07-3132. a) Siliciclastic content (wt.%); b) C_{org} (wt.%); c) biogenic carbonate (wt.%); d) biogenic opal (wt.%); e) C/N molar ratio; f) K/Si ratio; g) >150 µm fraction ("IRD" wt.%); h) magnetic susceptibility (SI), and alkenone concentration (µg/g). Vertical gray shading corresponds to basal sediments characterized by a diamicton facies. The three tephra layers (Mount Burney 1: MB1; Hudson 1: H1 and Mount Burney 2: MB2) are marked by vertical orange lines.

4.1. Holocene glacier variability

As we have described earlier, we use the fluctuations in the K/Si ratio to interpret glacial clay contribution (Fig. 5f) as well as increases in AR siliciclastics (Fig. 5e) as reflecting increased glacial erosion within the fjord catchment in the Andes around the Cordillera Darwin (Fig. 1). During the relatively early Holocene a very pronounced glacial clay input (K/Si > 1.5) centered at ~9.8 kyr BP accompanied by very high AR of siliciclastics (>1800 kg m^{-2} kyr^{-1}) and low AR of $_{terr}$OC (<5 kg m^{-2} kyr^{-1}) is observed in the central basin (Fig. 5). Concurrently, high freshwater contribution likely due to precipitation occurs between 11.5–8.5 kyr BP in the western sector of the Strait of Magellan, which is supported by high $_{terr}$OC AR in Lake Tamar (Lamy et al., 2010; Kilian and Lamy, 2012) (Fig. 6c). These findings could reflect high freshwater contribution due to warming (resulting in intense glacier melting and lower SST's) or even an abrupt proglacial lake drainage due to a destabilization of the moraine system in the central basin. Additional input of glacial clays during this period could also be attributed to strong erosion of exposed coastal terraces as a result of the marine transgression process operating in the area.

Between 8.5 and 5 kyr BP, AR of siliciclastics are relatively low with no major fluctuations (Fig. 5e) and the K/Si ratio indicate, in general, little glacial clay input (Fig. 5f). The accumulation rates of $_{terr}$OC show the same trend (Fig. 5d). These results allow to infer that during the mid-Holocene the central basin was less affected by glacier melting and the freshwater flux remained rather stable. This decreasing trend in AR of siliciclastics and $_{terr}$OC was also observed in the western area of the Strait of Magellan by Lamy et al. (2010) at site TML1 (Lake Tamar).

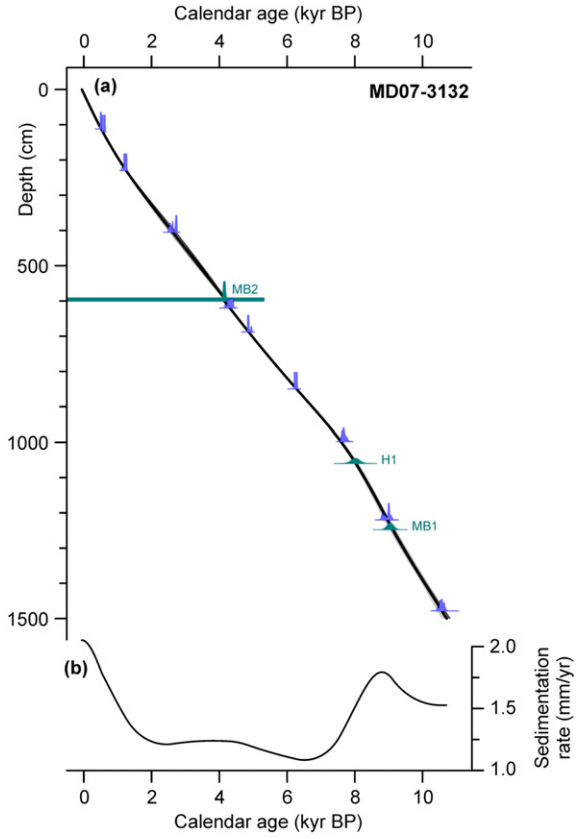

Fig. 4. CLAM age model (a) and sedimentation rates (b) of sediment core MD07-3132. The chronology is based on 10 AMS radiocarbon dates (blue; see Table 1) and three tephra layers (marked in green, MB1: 9050 ± 200 yr BP; H1: 8020 ± 250 yr BP and MB2: 4150 ± 50 yr BP; Kilian et al., 2003; Stern et al., 2008; Stern 2011). The deepest radiocarbon age was obtained at 1475 cm. Although the sediment core is 2173 cm long, the chronology was not extrapolated below 1475 cm due to a change in lithology, most likely representing very distinct sedimentary conditions (see Supplementary information, Figs. S1 and S2).

Finally, the in the late Holocene, between 3.2–2.2 kyr BP, $_{terr}$OC at our site presents high values, accompanied by a slight increase in glacial clay contribution. However, the latest Holocene (from 2 kyr BP to the present) was characterized by a rapid increase in the AR of siliciclastics and $_{terr}$OC, probably linked to an intensification of the freshwater flux derived from high precipitation.. Erosional processes triggered by Neoglacial glacier advances in the southern Andes (Wenzens, 2005; Glasser and Ghiglione, 2009) can explain these observations in our record. These appear to be contemporary with global glacier advances (Porter, 2000; Magny and Haas, 2004) in this epoch. Several paleoclimatic records from the western fjords (Kilian and Lamy, 2012; Kilian et al., 2013a, 2013b; Caniupán et al., 2014) and a precipitation record from a stalagmite at 53°S (Schimpf et al., 2011) indicate that these glacier advances occurred during comparatively warm phases of relatively high precipitation and were also significantly controlled by SWW-related accumulation changes (Kilian et al., 2013a). At the eastern fjords there is no clear evidence of glacier advances during the Neoglacial. However, at Lago Fagnano (Moy et al., 2008; 2011) a generally higher precipitation is recorded which can be explained by a higher amount of easterly-derived precipitation due to a weaker SWW (Kilian and Lamy, 2012).

In the southernmost Andes Holocene glacier advance phases are controlled by the interplay between accumulation (mainly SWW controlled: Lamy et al., 2010) and ablation. The latter reflects temperature changes which can be obtained from alkenone-based and ice core-derived paleotemperature (see data compilation Kilian and Lamy, 2012). Nevertheless, in areas influenced by glacier melting the surface water is not in equilibrium with air temperatures and alkenone derived SSTs may represent partly the release of colder water from ice melting. SST records from open ocean sites may better reflect regional air temperatures whereas fjord SSTs are overprinted by local seasonal processes (Caniupán et al., 2014). In fact, our results does not include a continuous alkenone SST's record for the early Holocene due the intermittence of alkenones in these sediments. Once that their presence is constant, alkenone SST reached ~9 °C at ~8.4 kyr BP to further show a pronounced increase towards ~11 °C at 8 kyr BP, and a second peak of ~10.5 °C at ~6 kyr BP. For the late Holocene, alkenone SST records from northern Patagonian fjords (Sepúlveda et al., 2009; Caniupán et al., 2014) suggest SST cooling between 3.5–2.5 kyr BP and during the Little Ice Age. The highest temperature value (10.9 °C) for the Late Holocene in our sediments occurs at ~2.1 kyr BP (Fig. 6g, blue line). This is followed by a drop to <8 °C with a short peak of 9.9 °C at 0.8 kyr BP, possibly related to the Medieval Warm Period.

4.2. Holocene marine transgression and coastline evolution: implications for salinity changes

The Cl/water% ratio obtained along MD07-3132 sediment core allowed reconstructing past changes in salinity and therefore in the freshwater flux (Fig. 5g; see Supplementary information, Figs. S3a and b; Kilian et al., 2013a, b). Between 10.5 and 8 kyr BP the Cl/Water % and AR of biogenic $CaCO_3$ (Fig. 6b and f, respectively) remain relatively low which may be partly linked to relatively high precipitation in the Andean mountain range as indicated by relatively high AR of $_{terr}$OC (Fig. 5d) and in Lake Tamar (Fig. 6c; Lamy et al., 2010). This can be also related with high glacial clay input as we discussed in the previous section. For the mid Holocene our sediments show that between 8.5 and 5 kyr BP, the Cl/Water % progressively increases towards the late Holocene in accordance with the marine transgression (Fig. 6d), and a warming trend (Fig. 6g blue line). It is also likely that the eastern entrance of the Strait of Magellan opened due to further sea level rise at that time ending with the complete isolation of Tierra del Fuego. During the late Holocene, the AR of CaCO3 significantly decreases between 3.2 and 2.2 kyr BP, suggesting a drop in salinity, although this is not clearly observed in the Cl/Water content ratio (Fig. 6 b, g). This event is also related with the rise in the AR of $_{terr}$OC and siliciclastics derived from intense freshwater flux described for the late Holocene in the former chapter. When we compare smooth data of glacioeustatic changes (Siddall et al., 2003) with the Cl/Water % fluctuations from our core we observe similar variability although the amplitude is more pronounced during the late Holocene. It is possible that a northward displacement and/or weakening of the SWWs could limit the eastward freshwater flow (Lamy et al., 2010) explaining the overall higher salinities and paleoproductivity during this period in our record. In the context of the marine transgression the interpretation of our results need to consider the interplay between isostasy, vertical tectonic crustal movements and eustasy. These processes defined the coastline evolution and partially the thermohaline structure of the water column in each fjord basin (Kilian et al., 2007a; Boyd et al., 2008). In Southern Patagonia an increase in coastline elevation reduced the vegetation area and enabled saltier water to reach the shallow coastal sites, leading to higher biogenic carbonate production (Kilian et al., 2007a). Furthermore, the interaction between Holocene glacier fluctuations and the marine transgression might have had consequences in the stability of outlet-glaciers at Cordillera Darwin since increasing coastline elevation transformed proglacial lakes into fjords. Simultaneously, our salinity-sensitive proxies suggest that the freshwater flux produced by meltwater influenced the biogenic production during the Holocene.

4.3. Productivity changes during the Holocene and the influence of freshwater flux

The results obtained on sediment record MD07-3132 include AR of $_{mar}$OC, biogenic carbonate, and biogenic opal as productivity proxies.

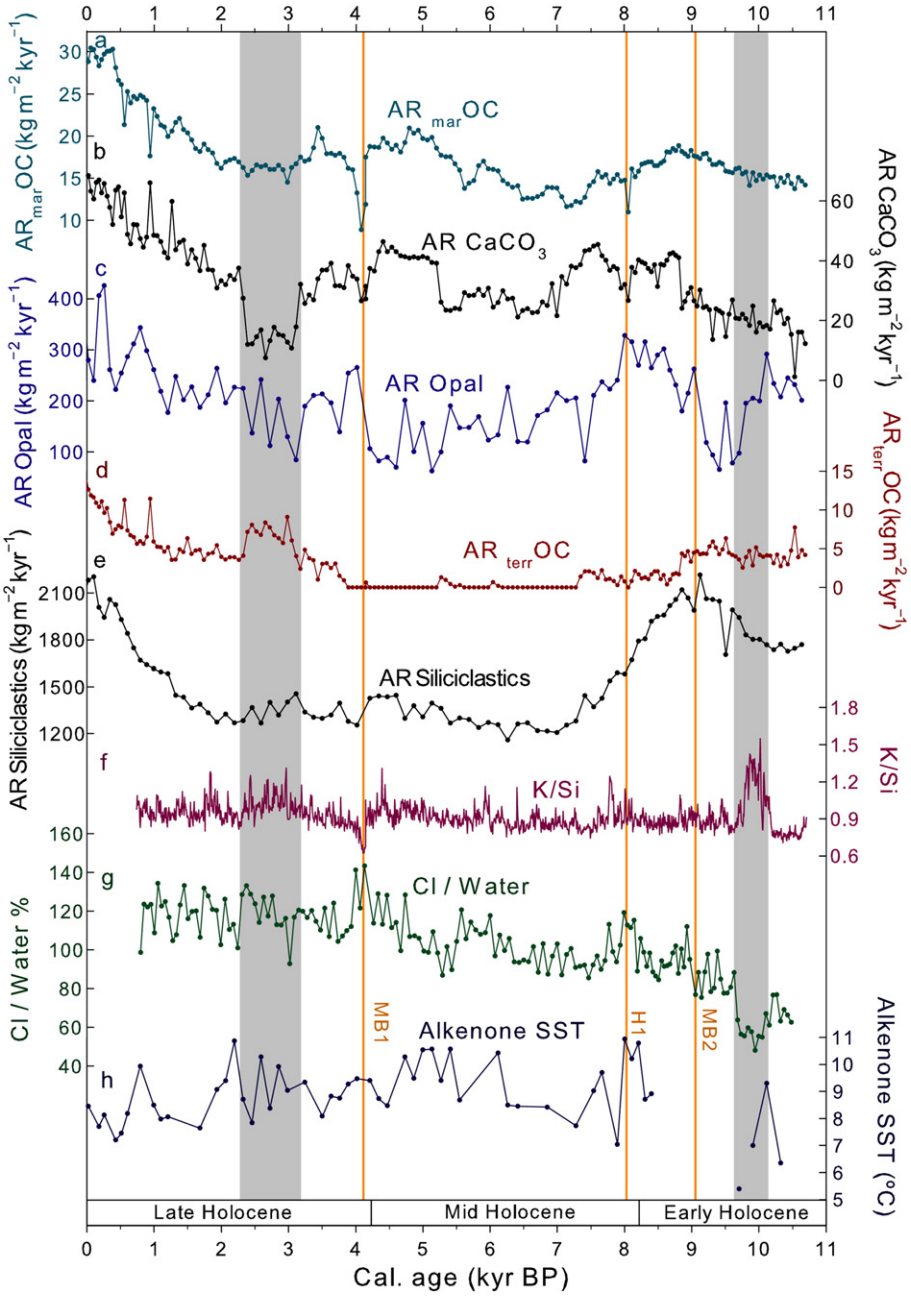

Fig. 5. Accumulation rates (AR) of biogenic production and inorganic proxies from core MD07-3132 during the past ~10.5 kyr BP. a) AR marine organic carbon (AR $_{mar}$OC); b) AR biogenic carbonate (AR $CaCO_3$); c) AR biogenic opal (AR Opal); d) AR terrestrial organic carbon (AR $_{terr}$OC); e) AR siliciclastic material (AR siliciclastics); f) K/Si ratio as proxy of glacial clay input; g) chlorine to water content ratio (Cl/Water %) as proxy of paleosalinity; and h) alkenone SST fluctuations. All ARs are expressed in kg m^{-2} kyr^{-1}. Tephras are marked by vertical orange lines. The vertical gray bars represent the periods of intense freshwater flux towards the central basin of the Strait of Magellan.

The early Holocene (between 10.5 and 8.2 kyr BP in our record) was characterized by very low AR of $_{mar}$OC, $CaCO_3$ and biogenic opal. For this time interval, our results are comparable with the findings of Harada et al. (2013) in the western Strait of Magellan at site PC-03 (Fig. 1) that reveal low ARs of organic carbon and total nitrogen, and alkenone contents between 13–9 kyr BP followed by a rapid increase at ~8 kyr BP. Lamy et al. (2010) also observed low AR of $CaCO_3$ (~30 kg m^{-2} kyr^{-1}) at site PALM2 located at the western fjords at the entrance of the Pacific Ocean.

Our sediments reveal the re-occurrence of alkenones at ~8.4 kyr BP (Fig. 3i), which were intermittent and even absent at the base of the core. This re-occurrence in addition to the increase in AR $CaCO_3$ (fluctuating between 20 and 40 kg m^{-2} kyr^{-1}; Fig. 6f) and in the chlorine ratio (Fig. 6b), and to the decline in the AR of $_{terr}$OC (Fig. 5d) point to a reduced freshwater supply and higher salinities at our core site in the Whiteside Channel after ~8.5 kyr BP. Since alkenones and $CaCO_3$ are derived from the biological synthesis of marine organisms, we infer that higher marine bioproductivity was at least partially related to the Holocene marine transgression.

During the late Holocene, all biogenic accumulation rates in sediment core MD07-3132 show a general increase paralleling a rise in chlorine ratio values. A sudden increase in the AR of $_{terr}$OC (Figs. 5d and 6c) points to an abrupt freshwater supply at 3–2.5 kyr BP that could explain the significantly reduced AR of $CaCO_3$ (a decline from 32 to 7 kg m^{-2} kyr^{-1}) at that time; (Fig. 6f). Thereafter, all the productivity proxies have a fast recovery, where high values of biogenic opal and

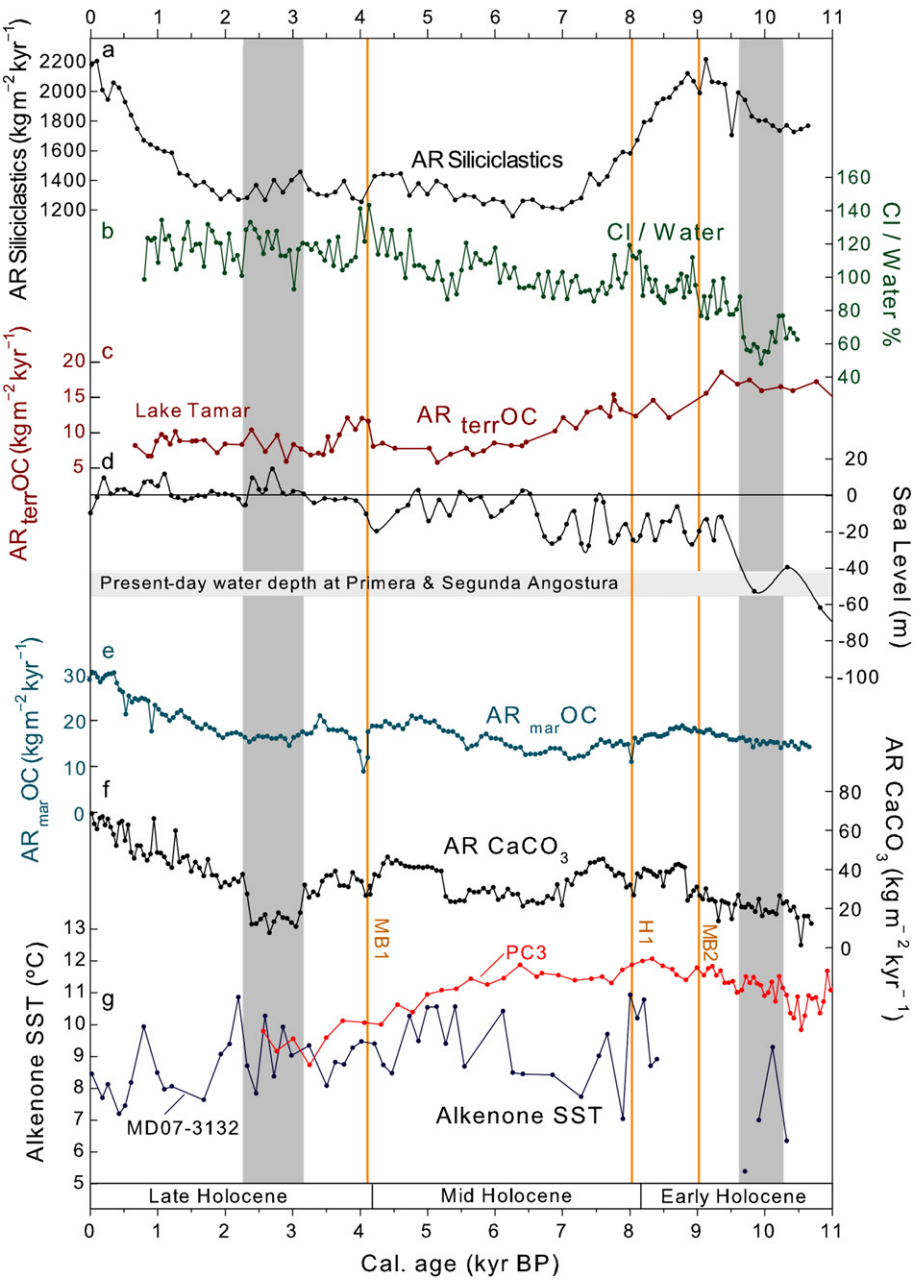

Fig. 6. Proxy records of paleoproductivity variations related to glacier fluctuations and changes in freshwater flux in the central basin of the Strait of Magellan during the past 10.5 kyr BP. a) AR siliciclastic material; b) chlorine to water content ratio (Cl/Water %); c) AR terrestrial organic carbon in Lake Tamar (Lamy et al., 2010); d) smoothed Holocene sea level fluctuations (Siddal et al., 2003); e) AR marine organic carbon; f) AR biogenic carbonate; g) Holocene alkenone-SST records from site MD07-3132 (this study, blue line) and site PC-03 at the western entrance of the Strait of Magellan near Cape Pilar at ~53°S (Harada et al., 2013; red line), The vertical gray bars represent the periods of intense freshwater flux towards the central basin of the Strait of Magellan.

$CaCO_3$ (Fig. 5b, c) contribute to the highest AR of $_{mar}$OC (Fig. 6e) once the coastal system was established.

At present, seasonal and shorter-term changes in estuarine stratification, influenced by the annual cycle in ice melting plus precipitation and events such as glacial-lake outburst floods (GLOF's; Dussaillant et al., 2009), can have profound influences on the marine ecosystem (González et al., 2013). For instance, in the last century Marinelli glacier has undergone the largest retreat yet documented in South America between 1992 and 2000, with values of 2.75 km × a^{-1} (Porter et al., 2003). High amounts of freshwater discharge influence the vertical distribution of nutrient concentration (Fig. 2, three lower panels) and light penetration, especially in glacier proximal areas. In general, spatial changes in surface light attenuation along the Patagonian fjord region are largely driven by glacier-derived freshwater inputs due to the release of glacial clay that remains suspended in the surface layer hampering photosynthetic processes (Silva, 2008; Aracena et al., 2011; Jacob et al., 2014) . This combination of nutrient and light limitation affects the physiological condition of phytoplankton (González et al., 2011, 2013) especially during the productive season (spring and summer). The vertical distribution of hydrographic conditions, from the Whiteside Channel to the east of Isla Dawson, where core MD07-3132 is located (Fig. 1), is characterized by nutrient-poor, cold freshwater indicating a strong influence of meltwater derived from glaciers of Cordillera Darwin (Fig. 2). Spring primary production values in two fjords of the Cordillera Darwin fjord system reveal that show Marinelli Fjord (distal) compared to the Brookes Fjord (proximal) (both belonging to the) showing 7 and

1.9 g C m^{-2} d^{-1}, respectively (Aracena et al., unpubl. data). These preliminary results reveal that a glacier distal fjord environment is more productive than a glacier proximal system.

This freshwater flux, which enhances salinity and turbidity gradients in the upper water column, may have generated critical conditions for planktic foraminifera (Bijma et al., 1990; Paasche et al., 1996) and coccolithophores, as suggested by their scarcity and even absence of alkenones below 1648 cm (i.e., in sediments older than 11 kyr BP). A compilation of modern data about spring primary production of the Chilean Patagonian fjords (41–55°S) showed that the lowest value was found in Caleta Tortel, Central Patagonia (91 mg C m^{-2} d^{-1}), a site heavily influenced by glacier melting and river discharge loaded with glacial sediments, which origin is in the confluence area of Northern and Southern Ice fields (Aracena et al., 2011). Also, we have compared spring primary production values obtained in Marinelli Fjord (distal) with Brookes Fjord (proximal) (both belonging to the Cordillera Darwin fjord system) showing 7 and 1.9 g C m^{-2} d^{-1}, respectively (Aracena et al., unpubl. data). These preliminary results reveal that a glacier distal fjord environment is more productive than a glacier proximal system. Additionally, at the western Patagonian fjords lower salinities occur during times of elevated precipitation. Stronger winds keep the low-salinity fjord waters inside and prevent the open marine influence on the fjord system, reducing biogenic carbonate production (Lamy et al., 2010). In the case of the Cordillera Darwin fjord system the morphology and orientation is different and may add another effect for glacier mass balance influencing the aquatic environment. If we extrapolate these modern observations to past changes in paleoproductivity for glacimarine environments of the Strait of Magellan basin, the interpretation of the biogeochemical proxies studied in core MD07-3132 is consistent with a negative effect of glacier melting on biological productivity, especially during the early Holocene.

5. Conclusions

Our results reveal that during the early Holocene productivity (based on AR of $_{mar}$OC, $CaCO_3$ and biogenic opal in the central basin of the Strait of Magellan) was very low, probably as a response to an intense period of freshwater influx which is supported by the high ARs of $_{terr}$OC and silicilastics and the high ratios of K/Si.

After ~8.5 kyr BP, the increase in the Cl/Water % and AR of biogenic $CaCO_3$ suggest reduced meltwater influence and higher salinities in the Whiteside Channel, conditions apparently favorable for fjord productivity. Glaciers may have been more stable during the mid-Holocene with no significant contribution of freshwater towards the central basin. On the other hand, this could have been complemented by the marine transgression operating in the area.

During the late Holocene, our results display the highest productivity of the entire record but major salinity changes are observed such as an abrupt decrease in the AR of biogenic $CaCO_3$ between 3 and 2.2 kyr BP. This phase points to an intense period of freshwater supply probably due to more precipitation and glacier advance. Finally, productivity had a fast recovery, where high values of AR Si_{OPAL} and $CaCO_3$ contributed to the highest AR of $_{mar}$OC.

The multi-proxy approach of our study suggests that in the central basin of the Strait of Magellan meltwater is one of the main factors controlling fjord bioproductivity, nutrient concentration, SSTs and salinities. In the current scenario of global warming, the increase of glacier melting could generate critical conditions for marine phytoplankton growth and less export production.

Acknowledgments

This work was funded by DFG grant Ki-456-/9-1 (to R. Kilian), DFG grants La-1273/3-2 and La-1273/5-1 (to F. Lamy), DFG grants AR 367/6-1 and AR 367/6-2 (to H. W. Arz), and the COPAS Center of the University of Concepción (grants # 150100007 and PFB-31). C. Aracena acknowledges doctoral scholarships from CONICYT #21060249 (2006–2010), CONA program CIMAR (3073-133-LE10), COPAS (2010–2011), and postdoctoral grant from FONDECYT 3130356. S. Bertrand acknowledges financial support from the Flemish Research Foundation (FWO 1215113N, Belgium). Carina Lange acknowledges fellowship from Hanse-Wissenschaftskolleg (Germany). We sincerely thank our personnel Lilian Nuñez, Alejandro Avila, and Victor Acuña for laboratory work, Eduardo Tejos for help with the ODV image, and the captain and crew of the R/V *Marion Dufresne* and IPEV for a very successful cruise.

Appendix A. Supplementary data

Supplementary data to this article can be found online at http://dx.doi.org/10.1016/j.palaeo.2015.06.023.

References

Acha, E.M., Mianzan, H.W., Guerrero, R., Favero, M., Bava, J., 2004. Marine fronts at the continental shelves of austral South America: physical and ecological processes. J. Mar. Syst. 44 (1–2), 83–105.

Antezana, T., 1999. Hydrographic features of Magellan and Fuegian inland passages and adjacent subantarctic waters. Sci. Mar. 63, 23–34.

Aracena, C., Lange, C.B., Iriarte, J., Rebolledo, L., Pantoja, S., 2011. Latitudinal patterns of export production recorded in surface sediments of the Chilean Patagonian fjords (41–55°S) as a response to water column productivity. Cont. Shelf Res. 31 (3–4), 340–355.

Araya-Vergara, J., 2008. The submarine geomorphology of the Chilean Patagonian fjords and piedmonts. In: Silva, N., Palma, S. (Eds.), Progress in the Oceanographic Knowledge of Chilean Interior Waters, From Puerto Montt to Cape Horn. Pontificia Universidad Católica de Valparaíso, Comité Oceanográfico Nacional, pp. 25–27.

Bertrand, S., Hughen, K.A., Sepúlveda, J., Pantoja, S., 2012. Geochemistry of surface sediments from the fjords of Northern Chilean Patagonia (44–47°S): Spatial variability and implications for paleoclimate reconstructions. Geochim. Cosmochim. Acta 76, 125–146.

Bianchi, C., Gersonde, R., 2004. Climate evolution at the last deglaciation: the role of the southern ocean. Earth Planet. Sci. Lett. 228, 407–424.

Bijma, J., Faber, W., Hemleben, C., 1990. Temperature and salinity limits for growth and survival of some planktonic foraminifers in laboratory cultures. J. Foraminifer. Res. 20 (2), 95–116.

Blaauw, M., 2010. Methods and code for 'classical' age-modelling of radiocarbon sequences. Quat. Geochronol. 5, 512–518.

Boyd, B., Anderson, J., Wellner, J., Fernández, R., 2008. The sedimentary record of glacial retreat, Marinelli Fjord, Patagonia: Regional correlations and climate ties. Mar. Geol. 255, 165–178.

Breuer, S., Kilian, R., Schörner, D., Weinrebe, W., Behrmann, J., Baeza, O., 2013. Glacial and tectonic control on fjord morphology and sediment deposition in the Magellan region (53°S), Chile. Mar. Geol. 346, 31–46.

Caniupán, A.M., Lamy, F., Lange, C.B., Kaiser, J., Arz, H.W., Kilian, R., Baeza Urrea, O., Aracena, C., Hebbeln, D., Kissel, C., Laj, C., Mollenhauer, G., Tiedemann, R., 2011. Millennial-scale sea surface temperature and Patagonian Ice Sheet changes off southernmost Chile (53°S) over the past ~ 60 kyr. Paleoceanography 26, PA3221. http://dx.doi.org/10.1029/2010PA002049.

Caniupán, A.M., Lamy, F., Lange, C.B., Kaiser, J., Kilian, R., Arz, H.W., León, T., Mollenhauer, G., Sandoval, S., De Pol-Holz, R., Pantoja, S., Wellnerf, J., Tiedemann, R., 2014. Holocene sea-surface temperature variability in the Chilean fjord region. Quat. Res. http://dx.doi.org/10.1016/j.yqres.2014.07.009.

Ch, Porter, Santana, A., 2003. Rapid 20th century retreat of ventisquero Marinelli in the Cordillera Darwin Ice Field. An. Ins. Patagonia 31, 17–26.

Dávila, P., Figueroa, D., Müller, E., 2002. Freshwater input into the coastal ocean and its relation with the salinity distribution off austral Chile (35°–55°S). Cont. Shelf Res. 22, 521–534.

Dussaillant, A., Benito, G., Buytaert, W., Carling, P., Meier, C., Espinoza, F., 2009. Repeated glacial-lake outburst floods in Patagonia: an increasing hazard? Natural Hazards 54, 469–481. http://dx.doi.org/10.1007/s11069-009-9479-8.

EPICA Community Members Augustin, Barbante, L., Barnes, C., Barnola, P.R.F., Bigler, J., Castellano, M., Cattani, E., Chappellaz, O., Dahl-Jensen, J., Delmonte, D., Dreyfus, B., Durand, G., Falourd, G., Fischer, S., Flückiger, H., Hansson, J., Huybrechts, M.E., Jugie, P., Johnsen, G., Jouzel, S.J., Kaufmann, J., Kipfstuhl, P., Lambert, J., Lipenkov, F., Littot, V.Y., Longinelli, G.C., Lorrain, A., Maggi, R., Masson-Delmotte, V., Miller, V., Mulvaney, H., Oerlemans, R., Oerter, J., Orombelli, H., Parrenin, G., Peel, F., Petit, D.A., Raynaud, J.R., Ritz, D., Ruth, C., Schwander, U., Siegenthaler, J., Souchez, U., Stauffer, R., Steffensen, B., Stenni, J.P., Stocker, B., Tabacco, T.F., Udisti, I.E., Wal, R., Broeke, R.S.W., Weiss, M., Wilhelms, J., Winther, F., Wolff, J.G., E. W., Zucchelli, M., 2004. Eight glacial cycles from an Antarctic ice core. Nature 429, 623–662.

Garreaud, R., Lopez, P., Minvielle, M., Rojas, M., 2013. Large Scale Control on the Patagonia Climate. J. Clim. 26, 215–230.

Glasser, N., Ghiglione, M., 2009. Structural, tectonic and glaciological controls on the evolution of fjord landscapes. Geomorphology 105, 291–302.

González, H., Castro, L., Daneri, G., Iriarte, J., Silva, N., Vargas, C., Giesecke, R., Sánchez, N., 2011. Seasonal plankton variability in Chilean Patagonia fjords: Carbon flow through

the pelagic food web of Aysen Fjord and plankton dynamics in the Moraleda Channel basin. Cont. Shelf Res. 31 (3–4), 225–243.
González, H., Castro, L., Daneri, G., Iriarte, J., Silva, N., Tapia, F., Teca, E., Vargas, C., 2013. Land–ocean gradient in haline stratification and its effects on plankton dynamics and trophic carbon fluxes in Chilean Patagonian fjords (47°–50°S). Prog. Oceanogr. 119, 32–47.
Harada, N., Ninnemann, U., Lange, C.B., Marchant, M., Sato, M., Ahagon, N., Pantoja, S., 2013. Deglacial–Holocene environmental changes at the Pacific entrance of the Strait of Magellan. Palaeogeogr. Palaeoclimatol. Palaeoecol. 375, 125–135.
Hogg, A.G., Hua, Q., Blackwell, P.G., Niu, M., Buck, C.E., Guilderson, T.P., Heaton, T.J., Palmer, J.G., Reimer, P.J., Reimer, R.W., Turney, C.S.M., Zimmerman, S.R.H., 2013. SHCal13 Southern Hemisphere Calibration, 0–50,000 years cal BP. Radiocarbon 55, 1889–1903.
Iriarte, J., González, H., Liu, K., Rivas, C., Valenzuela, C., 2007. Spatial and temporal variability of chlorophyll and primary productivity in surface waters of southern Chile (41.5–43° S). Estuar. Coast. Shelf Sci. 74, 471–480.
Jacob, B., Tapia, F., Daneri, G., Iriarte, J., Montero, P., 2014. Springtime size-fractionated primary production across hydrographic and PAR-light gradients in Chilean Patagonia (41–50°S). Prog. Oceanogr. http://dx.doi.org/10.1016/j.pocean.2014.08.003.
Kaiser, J., Lamy, F., Hebbeln, D., 2005. A 70-kyr sea surface temperature record off southern Chile (Ocean Drilling Program Site 1233). Paleoceanography 20. http://dx.doi.org/10.1029/2005PA001146.
Kilian, R., Lamy, F., 2012. A review of Glacial and Holocene paleoclimate records from southernmost Patagonia (49–55°S). Quat. Sci. Rev. 53, 1–23.
Kilian, R., Hohner, M., Biester, H., Wallrabe-Adams, H., Stern, Ch., 2003. Holocene peat and lake sediment tephra record from the southernmost Chilean Andes (53–55°S). Rev. Geol. Chile 30, 47–64.
Kilian, R., Baeza, O., Steinke, T., Arévalo, M., Ríos, C., Schneider, C., 2007a. Late Pleistocene to Holocene marine transgression and thermohaline control on sediment transport in the western Magellanes fjord system of Chile (53°S). Quat. Int. 161, 90–107.
Kilian, R., Schneider, C., Koch, J., Fesq-Martin, M., Biester, H., Casassa, G., Arévalo, M., Wendt, G., Baeza, O., Behrmann, J., 2007b. Palaeoecological constraint on late Glacial and Holocene ice retreat in the Southern Andes (53° S). Glob. Planet. Chang. 59, 49–66.
Kilian, R., Lamy, F., Arz, H., 2013a. Late Quaternary variations of the southern westerly wind belt and its influences on aquatic ecosystems and glacier extend within the southernmost Andes. Z. Dtsch. Ges. Geowiss. 164, 279–294.
Kilian, R., Baeza, O., Breuer, S., Ríos, F., Arz, H., Lamy, L., Wirtz, J., Baque, D., Korf, P., Kremer, K., Ríos, C., Mutschke, E., Michels, S., De Pohl-Holz, R., Arévalo, M., Wörner, G., Schneider, C., Casassa, G., 2013b. Late Glacial and Holocene paleogeographical and paleoecological evolution of the Seno Skyring and Otway fjord systems in the Magellan region. An. Ins. Patagonia 1 (2), 5–26.
Kissel, C., 2007a. The Shipboard Scientific Party. MD159-PACHIDERME-IMAGES XV. Data report, Les rapports de campagne à la mer, Réf. OCE/2007/01, Institut Paul-Emile Victo.
Kissel, C., 2007b. The Shipboard Scientific Party. MD159-PACHIDERME-IMAGES XV. Cruise report, Les rapports de campagne à la mer, Réf. OCE/2007/01, Institut Paul-Emile Victor.
Lamy, F., Kaiser, J., Arz, H., Ninnemann, U., Hebbeln, D., Timm, O., Timmermann, A., Toggweiler, J., 2007. Modulation of the bipolar seesaw in the southeast pacific during Termination 1. Earth Planet. Sci. Lett. 259, 400–413.
Lamy, F., Kilian, R., Arz, H., Francois, J., Kaiser, J., Prange, M., Steinke, T., 2010. Holocene changes in the position and intensity of the southern westerly wind belt. Nat. Geosci. 3, 695–699.
Magny, M., Haas, J.N., 2004. A major widespread climatic change around 5300 cal. yr BP at the time of the Alpine Iceman. J. Quat. Sci. 19 (5), 423–430.
McCulloch, R., Davies, S., 2001. Late-glacial and Holocene palaeoenvironmental change in the central Strait of Magellan, southern Patagonia. Palaeogeogr. Palaeoclimatol. Palaeoecol. 173, 143–173.
McCulloch, R., Bentley, M., Tipping, R.M., Clapperton, C., 2005a. Evidence for late-glacial ice dammed lakes in the central Strait of Magellan and Bahía Inútil, southernmost South America. Geogr. Ann. Ser. A Phys. Geogr. 87, 335–362.
McCulloch, R., Fogwill, C., Sugden, D., Bentley, M., Kubik, P., 2005b. Chronology of the last glaciation in central Strait of Magellan and Bahía Inútil, southernmost South America. Geogr. Ann. Ser. A Phys. Geogr. 87, 289–312.
Meyers, P.A., 2003. Applications of organic geochemistry to paleolimnological reconstructions,: A summary of examples from the Laurentian Great Lakes. Org. Geochem. 34, 261–289.
Mortlock, R., Froelich, P., 1989. A simple method for the rapid determination of biogenic opal in pelagic marine sediments. Deep-Sea Res. 36, 1415–1426.
Moy, C.M., Dunbar, R.B., Moreno, P., Francois, J.P., Villa-Martinez, R., Guilderson, T.P., Garreaud, R.D., 2008. Isotopic evidence for hydrologic change related to the westerlies in SW Patagonia, Chile, during the last millennium. Quat. Sci. Rev. 27 (13–14), 1335–1349.
Moy, C.M., Dunbar, R.B., Guilderson, T.P., Waldmann, N., Mucciarone, D.A., Recasens, C., Ariztegui, D., Austin, J.A., Anselmetti, F.S., 2011. A geochemical and sedimentary record of high southern latitude Holocene climate evolution from Lago Fagnano, Tierra del Fuego. Earth Planet. Sci. Lett. 302 (1–2), 1–13.
Müller, P., Schneider, R., 1993. An automated leaching method for the determination of opal in sediments and particulate matter. Deep-Sea Res. 40, 425–444.
Paasche, E., Brubak, S., Skattebøl, S., Young, J., Green, J., 1996. Growth and calcification in the coccolithophorid *Emiliania huxleyi* (Haptophyceae) at low salinities. Phycologia 35 (5), 394–403.
Perdue, E., Koprivnjak, J., 2007. Using the C/N ratio to estimate terrigenous inputs of organic matter to aquatic environments. Estuar. Coast. Shelf Sci. 73, 65–72.
Pizarro, G., Iriarte, J., Montecino, V., Blanco, J., Guzmán, L., 2000. Distribución de la biomasa fitoplanctónica y productividad primaria máxima de fiordos y canales australes (47°–50° S) en octubre de 1996. Comité Oceanográfico Nacional 23 pp. 25–48.
Porter, Ch., 2000. Onset of Neoglaciation in the Southern Hemisphere. J. Quat. Sci. 15 (4), 395–408.
Prahl, F., Wakeham, S., 1987. Calibration of unsaturation patterns in long-chain ketone compositions for palaeotemperature assessment. Nature 330, 367–369.
Ritcher, T., Van der Gaast, S., Koster, B., Vaars, A., Gieles, R., De Stigter, H., De Hass, H., Weering, T., 2006. The Avaatech XRF Core Scanner: Technical description and applications to NE Atlantic sediments. In: Rothwell, R. (Ed.), New Techniques in sediment core analysis. Geological Society of London Special Publication 267, pp. 39–50.
Saggiomo, V., Goffart, A., Carrada, G., Hecq, J., 1994. Spatial patterns of phytoplanktonic pigments and primary production in a semi-enclosed periantarctic ecosystem: the Straits of Magellan. J. Mar. Syst. 5, 119–142.
Schimpf, D., Kilian, R., Kronz, A., Simon, K., Spötl, C., Wörner, G., Deininger, M., Mangini, A., 2011. The significance of chemical, isotopic, and detrital components in three coeval stalagmites from the superhumid southernmost Andes (53° S) as high-resolution palaeo-climate proxies. Quat. Sci. Rev. 30, 443–459.
Schneider, C., Kilian, R., Santana, A., Butorovic, N., Casassa, G., 2003. Weather observations across the southern Andes at 53°S. Phys. Geogr. 24, 97–119.
Sepúlveda, J., Pantoja, S., Hughen, K.A., Bertrand, S., Figueroa, D., León, T., Drenzek, J., Lange, C.B., 2009. Late Holocene sea-surface temperature and precipitation variability in northern Patagonia, Chile (Jacaf Fjord, 44°S). Quat. Res. 72, 400–409.
SERNAGEOMIN, 2003. Mapa Geológico de Chile: versión digital. Servicio Nacional de Geología y Minería, Chile.
Siani, G., Michel, E., De Pol-Holz, R., De Vries, T., Lamy, F., Carel, M., Isguder, G., Dewilde, F., Lourantou, A., 2013. Carbon isotope records reveal precise timing of enhanced Southern Ocean upwelling during the last deglaciation. Nat. Commun. 4, 2758. http://dx.doi.org/10.1038/ncomms3758.
Siddall, M., Rohling, E.J., Almogi-Labin, A., Hemleben, Ch., Meischner, D., Schmelzer, D.A., Smeed, D., 2003. Sea level fluctuations during the last glacial cycle. Nature 423, 853–858.
Sievers, H.A., Silva, N., 2008. Water masses and circulation in austral Chilean channels and fjords. In: Silva, N., Palma, S. (Eds.), Comité Oceanográfico Nacional-Pontificia Universidad Católica de Valparaíso, pp. 53–58.
Silva, N., 2008. Physical and chemical characteristics of the surface sediments in the austral Chilean channels and fjords. In: Silva, N., Palma, S. (Eds.), Progress in the oceanographic knowledge of Chilean interior waters, from Puerto Montt to Cape Horn. Comité Oceanográfico Nacional-Pontificia Universidad Católica de Valparaíso, Valparaíso, pp. 69–75.
Stern, C.R., 2008. Holocene tephrochronology record of large explosive eruptions in the southernmost Patagonia Andes. Bull. Volcanol. 70, 435–454.
Sugden, D., Bentley, M., Fogwill, M., Hulton, N., McCulloch, R., Purves, R., 2005. Late-glacial glacier events in southernmost South America: a blend of 'northern' and 'southern' hemispheric climatic signals? Geogr. Ann. 87 A (2), 273–288.
Torres, R., Frangópulos, M., Hamamé, M., Montecino, V., Maureira, C., Reid, B., Valle-Levinson, A., Blanco, J., 2011. Nitrate to silicate ratio variability and the composition of micro-phytoplankton blooms in the inner-fjord of Seno Ballena (Strait of Magellan, 54°S). Cont. Shelf Res. 31 (3–4), 244–253.
Torres, R., Silva, N., Reid, B., Frangopulos, M., 2014. Silicic acid enrichment of subantarctic surface water from continental inputs along the Patagonian archipelago interior sea (41–56° S). Prog. Oceanogr. 129, 50–61.
Valdenegro, A., Silva, N., 2003. Caracterización oceanográfica física y química de la zona de canales y fiordos australes de Chile entre el estrecho de Magallanes y Cabo de Hornos (CIMAR 3 FIORDOS). Cienc. Tecnol. Mar. 26 (9), 19–60.
Valle-Levinson, A., Blanco, J., Frangópulos, M., 2006. Hydrography and frontogenesis in a glacial fjord off the Strait of Magellan. Ocean Dyn. 56, 217–227.
Walker, M.J.C., Berkelhammer, M., Björck, S., Cwynar, L.C., Fisher, D.A., Long, A.J., Lowe, J.J., Newnham, R.M., Rasmussen, S.O., Wiess, H., 2012. Formal subdivision of the Holocene Series/Epoch: a Discussion Paper by a Working Group of INTIMATE (Integration of ice-core, marine and terrestrial records) and the Subcommission on Quaternary Stratigraphy (International Commission on Stratigraphy). J. Quat. Sci. 27 (7), 649–659.
Wenzens, G., 2005. Glacier advances east of the Southern Andes between the Last Glacial maximum and 5,000 BP compared with lake terraces of the endorrheic Lago Cardiel (49°S, Patagonia, Argentina). Z. Geomorphol. 49 (4), 433–454.